Eur. Phys. J. C 49, 489–497 (2007)
DOI 10.1140/epjc/s10052-006-0161-y

THE EUROPEAN PHYSICAL JOURNAL C

Regular Article – Experimental Physics

Measurement of the top-Higgs Yukawa coupling at a linear e^+e^- collider

A. Gay[a]

Institut Pluridisciplinaire Hubert Curien, 23 rue du Loess, BP 20, 67037 Strasbourg, France

Received: 5 September 2006 / Revised version: 12 October 2006 /
Published online: 18 November 2006 –

Abstract. Understanding the mechanism of electroweak symmetry breaking and the origin of boson and fermion masses is among the most pressing questions raised in contemporary particle physics. If these issues involve one (several) Higgs boson(s), a precise measurement of all its (their) properties will be of prime importance. Among those, the Higgs coupling to matter fermions (the Yukawa coupling). At a linear collider, the process $e^+e^- \to t\bar{t}H$ will allow a direct measurement of the top-Higgs Yukawa coupling. We present a realistic feasibility study of the measurement in the context of the TESLA collider. Four channels are studied and the analysis is repeated for several Higgs mass values within the range 120–200 GeV/c^2.

PACS. 13.66.Jn; 14.65.Ha; 14.80.Bn

1 Introduction

The gauge sector of electroweak interactions has been checked to coincide with the standard model (SM) prediction to the per-mil level, at LEP and SLC. On the contrary, there is no direct experimental evidence for the Higgs mechanism, supposed to be responsible for electroweak symmetry breaking and the generation of masses. Direct search of the Higgs boson at LEP yields the lower limit [1]: $M_{\mathrm{H}} > 114.4\,\mathrm{GeV/c^2}$ at 95% CL. Precision measurements on the other hand give [2]: $M_{\mathrm{H}} \lesssim 200\,\mathrm{GeV}/c^2$ at 95% CL. Once a Higgs particle is found, if ever, all its properties should be measured precisely to completely characterise the Higgs mechanism. Among those, the coupling of the Higgs boson to fermions (the Yukawa coupling), which is supposed to scale with the fermion mass: $g_{ffH} = \frac{m_f}{v}$ where g_{ffH} is the Yukawa coupling of a fermion f of mass m_f and v is the vacuum expectation value of the Higgs field, $v = (\sqrt{2}G_{\mathrm{F}})^{-1/2} \approx 246\,\mathrm{GeV}$.

The top quark is the heaviest fermion, thus the top-Higgs Yukawa coupling should be the easiest to measure. If $M_{\mathrm{H}} > 2 * m_t$, this parameter can be measured through the branching ratio of the Higgs boson decay into a pair of top quarks. Otherwise, i.e. for lower values of the Higgs boson mass, the process $e^+e^- \to t\bar{t}H$ allows a direct measurement of this coupling.

Feasibility studies of the measurement of the top-Higgs Yukawa coupling via the process $e^+e^- \to t\bar{t}H$ at a linear collider (LC) have already been performed [3, 4] for a Higgs boson mass of 100–130 GeV/c^2. This is the most favourable case (taking into account the lower mass bound) as the cross-section of this process decreases with increasing Higgs boson mass and as a Higgs boson of such a mass decays predominantly to a pair of b quarks, allowing a very effective signal and background separation using b-tagging algorithms. One of the studies ([4]) showed that a multivariate analysis was essential to get a precise result. We repeated this work and extended it up to $M_{\mathrm{H}} = 150\,\mathrm{GeV}/c^2$. When $M_{\mathrm{H}} \gtrsim 135\,\mathrm{GeV}/c^2$, the $H \to W^+W^-$ decay mode dominates. This channel was also studied, for masses up to 200 GeV/c^2.

More details on this analysis can be found in [5, 6].

2 Extracting $g_{tt\,H}$

2.1 The process $e^+e^- \to t\bar{t}H$

The lowest order Feynman diagrams contributing to the $e^+e^- \to t\bar{t}H$ process are shown in Fig. 1. As the diagram where the Higgs boson is radiated from the Z boson modifies only slightly the cross-section [4], the following relation is verified to a good approximation: $\sigma_{e^+e^- \to t\bar{t}H} \propto g^2_{tt\,H}$.

For this work, we assumed: $m_t = 175\,\mathrm{GeV}/c^2$ and $\mathrm{BR}(t \to Wb) = 100\%$. The branching ratios of the Higgs boson decays considered in this study are shown in Table 1.

For the lowest Higgs mass values allowed, competitive results with those obtained at the LHC could be achieved at the starting energy of the LC (500 GeV). For example, a statistical precision of 10% for $M_{\mathrm{H}} = 120\,\mathrm{GeV}/c^2$ is foreseen in [9]. However, centre-of-mass energies well above the kinematic limit of the process will give much better results

[a] e-mail: arnaud.gay@ires.in2p3.fr;
Present address: Rutherford Appleton Laboratory, Chilton, Didcot, Oxon, UK, OX11 0QX

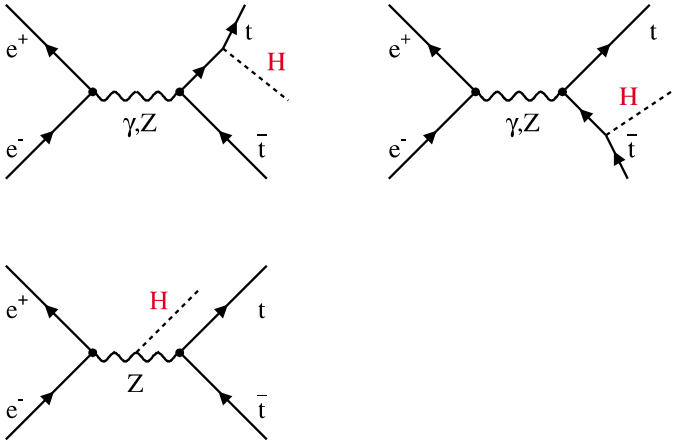

Fig. 1. Lowest order Feynman diagrams of the process $e^+e^- \to t\bar{t}H$

Table 1. Higgs branching ratios for the $H \to b\bar{b}$ and $H \to W^+W^-$ modes (as given by HDECAY [7]) and cross-section at lowest order of the process $e^+e^- \to t\bar{t}H$ (as given by CompHEP [8]), for various Higgs mass values and for $\sqrt{s} = 800$ GeV. In the calculation of the cross-section, initial state radiation and beamstrahlung were taken into account

M_{H} (GeV/c^2)	BR($H \to b\bar{b}$)	BR($H \to W^+W^-$)	σ (fb)
120	67%	13%	2.50
130	51%	30%	2.17
140	33%	50%	1.88
150	16%	70%	1.64
160	3.1%	92%	1.44
170	0.76%	97%	1.25
180	0.48%	93%	1.09
200	0.23%	73%	0.80

and will be needed in any case for the higher Higgs mass values. A run at 800 GeV being a very likely possibility for the LC, this will be the default value of our study. The lowest order cross-sections of the process are shown in Table 1 for the Higgs mass range considered.

At a centre-of-mass energy of 800 GeV, the $\mathcal{O}(\alpha_s)$ corrections to the $e^+e^- \to t\bar{t}H$ process affect the total cross-section [10–13] by less than 5% and were thus neglected in this study.

2.2 Measurement of $g_{tt\,H}$

For a particular analysis yielding a selection efficiency for the signal $\epsilon_{\mathrm{sel}}^{\mathrm{signal}}$, a purity of the selected sample $\rho_{\mathrm{sel}}^{\mathrm{sample}}$ and assuming an integrated luminosity L, the statistical and systematic uncertainties on the measurement of $g_{tt\,H}$ can be expressed as follows:

$$\left(\frac{\Delta g_{tt\,H}}{g_{tt\,H}}\right)_{\mathrm{stat}} \approx \frac{1}{S_{\mathrm{stat}}(g^2_{tt\,H})\sqrt{\epsilon_{\mathrm{sel}}^{\mathrm{signal}}\rho_{\mathrm{sel}}^{\mathrm{sample}}L}} \quad (1)$$

$$\left(\frac{\Delta g_{tt\,H}}{g_{tt\,H}}\right)_{\mathrm{syst}} \approx \frac{1}{S_{\mathrm{syst}}(g^2_{tt\,H})}\frac{1-\rho_{\mathrm{sel}}^{\mathrm{sample}}}{\rho_{\mathrm{sel}}^{\mathrm{sample}}}\frac{\Delta\sigma_{\mathrm{BG}}^{\mathrm{eff}}}{\sigma_{\mathrm{BG}}^{\mathrm{eff}}} \quad (2)$$

The default value for L assumed through the whole study is 1000 fb^{-1}. This large value is quite essential to maintain the statistical uncertainty at the level of a few per-cent. $\frac{\Delta\sigma_{\mathrm{BG}}^{\mathrm{eff}}}{\sigma_{\mathrm{BG}}^{\mathrm{eff}}}$ is the relative uncertainty on the residual background normalisation, which comes dominantly from $t\bar{t}$ pairs. It is mostly due to badly known differential cross-sections in weakly populated phase space corners. It is sizeable and moreover difficult to estimate. However, $t\bar{t}$ pairs will be copiously produced at the LC, allowing a complete characterisation of them. For example, studying these pairs during a run at an energy where the $t\bar{t}H$ process is negligible will allow to improve their simulation by event generators. Therefore, this uncertainty should not exceed 10%. We will thus repeat the analysis for two values of this uncertainty, 10% and 5%. In the systematic uncertainty, we just take into account the one which arises from the effective background normalisation since it is by far the largest one among those we can estimate now.

The sensitivity factors S_{stat} and S_{syst} in (1) and (2) express the dependence of the cross-section on the coupling squared:

$$S_{\mathrm{stat}}(g^2_{tt\,H}) = \frac{1}{\sqrt{\sigma_{t\bar{t}H}}}\left|\frac{\mathrm{d}\sigma_{t\bar{t}H}}{\mathrm{d}g^2_{tt\,H}}\right| \quad (3)$$

$$S_{\mathrm{syst}}(g^2_{tt\,H}) = \frac{1}{\sigma_{t\bar{t}H}}\left|\frac{\mathrm{d}\sigma_{t\bar{t}H}}{\mathrm{d}g^2_{tt\,H}}\right| \quad (4)$$

As the contribution from Higgs radiation off the Z to the signal cross-section is very small (see Sect. 2.1), we can write:

$$\sigma_{t\bar{t}H} \approx g^2_{tt\,H}F(M_{\mathrm{H}}, m_t, s) \quad (5)$$

And thus:

$$\frac{\mathrm{d}\sigma_{t\bar{t}H}}{\mathrm{d}g^2_{tt\,H}} \approx F(M_{\mathrm{H}}, m_t, s) \approx \frac{\sigma_{t\bar{t}H}}{g^2_{tt\,H}} \quad (6)$$

where s is the squared collision energy and F a function only dependent on M_{H}, m_t and s.
The sensitivity factors eventually read:

$$S_{\mathrm{stat}}(g^2_{tt\,H}) = \frac{\sqrt{\sigma_{t\bar{t}H}}}{g^2_{tt\,H}} \quad (7)$$

$$S_{\mathrm{syst}}(g^2_{tt\,H}) = \frac{1}{g^2_{tt\,H}} \quad (8)$$

3 Analysis and simulation

3.1 Background

The background processes considered in the analysis are listed in Table 2, together with their cross-sections.

The processes $e^+e^- \to q\bar{q}$ and $e^+e^- \to W^+W^-$ exhibit a very different topology from the signal, however, their

Table 2. Background cross-sections for $\sqrt{s} = 800\,\text{GeV}$ from CompHEP. Initial state radiation and beamstrahlung are taken into account

Elementary process	σ (fb)
$e^+e^- \to q\overline{q}$	1557.7
$e^+e^- \to t\overline{t}$	297.3
$e^+e^- \to W^+W^-$	4298
$e^+e^- \to ZZ$	239.8
$e^+e^- \to t\overline{t}Z$	4.3

huge cross-section (two or three orders of magnitude above the signal cross-section) forbids to neglect them.

Although its cross section is much lower, the above statements hold for the process $e^+e^- \to ZZ$.

The process $e^+e^- \to t\overline{t}Z$ and its cross section are very close to those of the signal.

Finally, the process $e^+e^- \to t\overline{t}$ has a rather large cross-section and will often mimic the signal. It will be the main background for every channel studied here.

3.2 Generation of events and simulation of the detector

The $t\overline{t}H$ and $t\overline{t}Z$ partonic events were generated with CompHEP V.41.10. This program allows to include the initial state radiation and the beamstrahlung. These events were then treated with PYTHIA V.6.158 [14] for hadronization, decay and final state radiation. Other backgrounds were generated with PYTHIA V.6.158. In this case, the initial state radiation was considered in the structure function approach and the beamstrahlung was implemented with CIRCE [15].

The events were further processed by SIMDET V.4 [16], the fast simulation program of the TESLA [17] detector, in order to take into account detector and event reconstruction effects.

3.3 *b*-tagging

The *b*-tagging is an essential tool for this analysis. *b* and *c*-tagging algorithms developed for LEP and SLC experiments were adapted to TESLA [18, 19] and made available with the fast simulation of the detector [20]. Various algorithms are combined, including the SLD-ZVTOP vertex finder, in a neural network. One of the outputs is the b-probability of a jet.

In the following, $P_b^{\text{jet}}(i)$ is the probability of the i^{th} jet of an event to be a *b*-jet, the $P_b^{\text{jet}}(i)$ values of an event being sorted out in decreasing order, i.e. from the most *b*-like to the least *b*-like.

3.4 Neural network analysis

A neural network is used to optimize the selection of events. We used the MLPfit program [21], a multi-layer perceptron with error backpropagation.

4 Study of the $H \to b\overline{b}$ decay mode

When the Higgs boson decays into $b\overline{b}$ pairs, 3 classes of final states occur. We only considered the two classes with the highest branching ratios: the semileptonic final state ($t\overline{t} \to W^+bW^-\overline{b} \to 2b2ql\nu$ with $\text{BR}(t\overline{t} \to 2b2ql\nu) \approx 43.9\%$) and the hadronic final state ($t\overline{t} \to W^+bW^-\overline{b} \to 2b4q$ with $\text{BR}(t\overline{t} \to 2b4q) \approx 45.6\%$). These two channels are characterized by a large particle and jet multiplicity and an isotropic topology. The presence of four *b*-jets will allow the construction of very discriminating variables. However, the event rate is really tiny in comparison with the background and the very crowded environnement will degrade clustering and *b*-tagging algorithms and will make invariant mass constraints less effective. Furthermore, hard gluon radiation combined with gluon splitting to $b\overline{b}$ will often allow the background events to fake the signal.

For both channels, a preselection sequential procedure is first applied in order to remove most of the background, while keeping a high selection efficiency for the signal. A neural network analysis will then be performed in order to optimally use the information contained in the distributions of the final state characteristics. The analysis will be repeated for the following Higgs boson masses: $120\,\text{GeV}/c^2$, $130\,\text{GeV}/c^2$, $140\,\text{GeV}/c^2$ and $150\,\text{GeV}/c^2$. As the distributions hardly change in this mass window, the same procedure will be applied for each value of the Higgs boson mass.

4.1 Semileptonic channel

The final state follows from the process: $e^+e^- \to t\overline{t}H \to W^+bW^-\overline{b}b\overline{b} \to 4b2ql\nu$. This channel is thus characterized by 4 *b*-jets, 2 light quark jets, one prompt lepton and missing 4-momentum. As compared to the hadronic channel, the final state is cleaner and the presence of an isolated lepton together with missing 4-momentum will allow to construct powerful selection variables.

4.1.1 Sequential analysis

First, we require the presence in the event of at least one charged lepton (a $\mu^\pm$ or a $e^\pm$). Then, we request:

- $500\,\text{GeV}/c^2 <$ Total visible mass $< 750\,\text{GeV}/c^2$.
- Total multiplicity ≥ 110.
- Number of jets (including possible isolated leptons; JADE algorithm with $y_{\text{cut}} = 1.10^{-3}$) ≥ 7.
- Thrust ≤ 0.85.
- Light jet mass $\geq 50\,\text{GeV}/c^2$.
- Heavy jet mass $\geq 150\,\text{GeV}/c^2$.
- Fox–Wolfram moment $h10 \leq 0.2$.
- Fox–Wolfram moment $h20 \leq 0.6$.
- Fox–Wolfram moment $h30 \leq 0.4$.
- Fox–Wolfram moment $h40 \leq 0.5$.

Next, an energetic and isolated charged lepton has to be identified. Among all the charged leptons ($\mu^\pm$ and $e^\pm$) reconstructed by the detector, the one which maximises the quantity $E_l * (1 - \cos\theta)$ is chosen, E_l being the energy of the lepton and θ the angle between its direction and that

of the closest jet when we force the rest of particles in a 6 jet configuration (with JADE). This procedure allows to choose a lepton from a leptonic decay of a W rather than from a B (or D) -meson decay which tends to be less energetic and isolated.

Once the lepton is tagged, the remaining particles are forced into 6 jets with the JADE algorithm. We then flavour-tag the jets and finally we require:

- Mininum jet multiplicity ≥ 3.
- $\sum_{i=1}^{4} P_b^{\rm jet}(i) \geq 1$.

4.1.2 Neural network analysis

A neural network is then trained with the following variables:

- The total visible mass.
- The number of jets (including possible isolated leptons; JADE algorithm with $y_{\rm cut} = 1.10^{-3}$).
- The thrust.
- The aplanarity.
- The second Fox–Wolfram moment $h20$.
- $\sum_{i=1}^{4} P_b^{\rm jet}(i)$.
- $E_{\rm max}^{\rm jet} - E_{\rm min}^{\rm jet}$.
- The energy of the tagged lepton.
- The invariant mass of the system made of the lepton and the missing momentum.
- The cosine of the angle between the tagged lepton and the closest jet directions.

Apart from the 5 first variables, all of them were calculated once the event was forced to the lepton tagged plus 6 jet configuration.

Once the neural network is trained, its weights are optimized for the separation of signal from background events. The distribution of the neural network output for these 2 classes of events is shown in Fig. 2 when $M_{\rm H} = 120\,{\rm GeV}/c^2$. From this figure, we observe that the separation is quite effective. However, due to the tiny cross-section of the signal process, the purity of the selected sample and the selection efficiency for the signal will be small and, eventually, the accuracy on the measurement of $g_{tt\,H}$ will be limited accordingly ((1) and (2)).

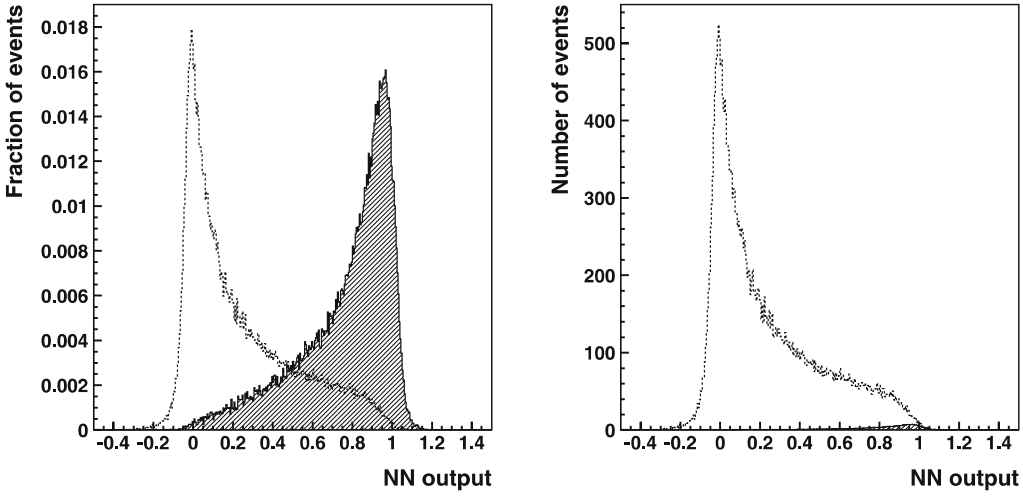

Fig. 2. The $H \to b\overline{b}$ semileptonic channel: neural network output. *Left* [*right*], the *signal* (*solid line*) and the *background* (*dashed line*) are normalised to 1 [the expected number of events]. The signal is shown for $M_{\rm H} = 120\,{\rm GeV/c^2}$

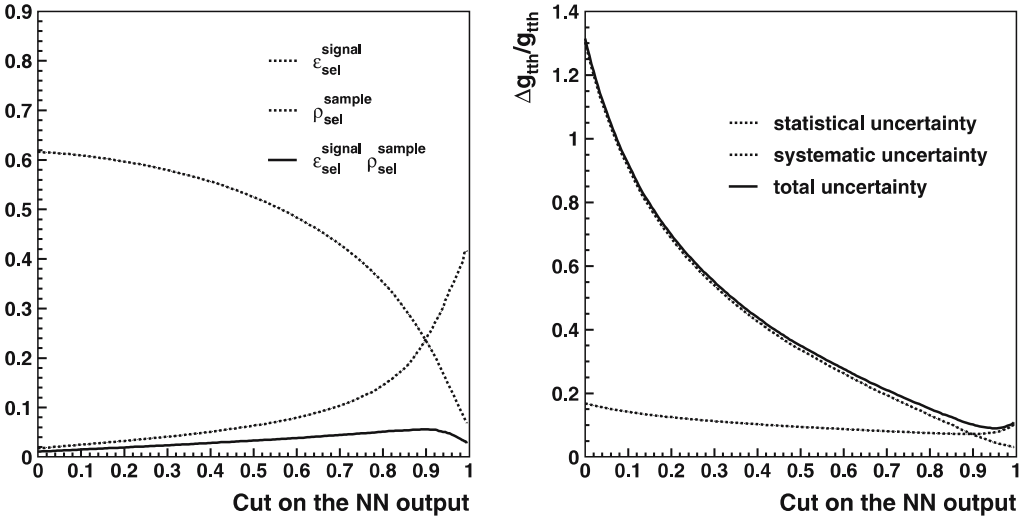

Fig. 3. The $H \to b\overline{b}$ semileptonic channel: (*left*) selection efficiency, purity and their product, (*right*) statistical, systematic and total uncertainties on the measurement of $g_{tt\,H}$ as functions of the value of the cut on the neural network output for $\frac{\Delta\sigma_{\rm BG}^{\rm eff}}{\sigma_{\rm BG}^{\rm eff}} = 5\%$ and $M_{\rm H} = 120\,{\rm GeV/c^2}$

4.1.3 Results

The next step consists of applying a cut on the neural network output to further separate the signal from the background. The cut value is chosen such that it minimises the quadratic sum of the statistical and systematic uncertainties. The value of this optimal cut depends on the assumption made for the value of the uncertainty on the residual background normalisation and on the number of signal events, which in turn depends on the Higgs boson mass.

The evolution of the selection efficiency of the signal $\epsilon_{\rm sel}^{\rm signal}$, the purity of the selected sample $\rho_{\rm sel}^{\rm sample}$, their products, the statistical, systematic and total uncertainties are shown in Fig. 3 as a function of the cut on the neural network output, for the case where $M_{\rm H} = 120\,{\rm GeV}/c^2$ and $\frac{\Delta\sigma_{\rm BG}^{\rm eff}}{\sigma_{\rm BG}^{\rm eff}} = 5\%$. As we increase the cut, the purity gets higher and its derivative increases. The systematic uncertainty behaves in the same way as $\frac{1-\rho_{\rm sel}^{\rm sample}}{\rho_{\rm sel}^{\rm sample}}$. It is a decreasing function of ρ, which varies fast for values of ρ close to 0 and less as ρ increases. The evolution of the selection efficiency is opposite to the one of the purity. Their product has thus a small variation. It however increases until a particular cut value (0.92 for this case). The statistical uncertainty will thus slowly decrease until this cut value. A higher cut value generates a sharp drop of the efficiency and a degradation of the statistical uncertainty. Eventually, the optimal cut is about 0.95 for the case under study.

The resolutions on $g_{tt\,H}$ (Fig. 4) range from 9.1% (11.7%) to 48.7% (65.9%) for $\frac{\Delta\sigma_{\rm BG}^{\rm eff}}{\sigma_{\rm BG}^{\rm eff}} = 5\%$ (10%).

4.2 Hadronic channel

The final state follows from the process: $e^+e^- \to t\bar{t}H \to W^+bW^-\bar{b}b\bar{b} \to 4b4q$. This channel is thus characterized by 4 b-jets and 4 light quark jets. As compared to the semileptonic channel, the environnement is still more crowded, thus deteriorating the event reconstruction.

4.2.1 Sequential analysis

We first require:

- Total visible mass $\geq 560\,{\rm GeV}/c^2$.
- Total multiplicity ≥ 120.
- Number of jets (including possible isolated leptons; JADE algorithm with $y_{\rm cut} = 1.10^{-3}$) ≥ 7.
- Thrust ≤ 0.85.

The events satisfying these requirements are forced in a 8 jet configuration (using JADE) and a second set of criteria is then applied:

- Minimum jet multiplicity > 1.
- Minimum dijet invariant mass $\geq 15\,{\rm GeV}/c^2$.
- $E_{\rm min}^{\rm jet} \geq 20\,{\rm GeV}$.

4.2.2 Neural network analysis

A neural network is then trained with the following variables:

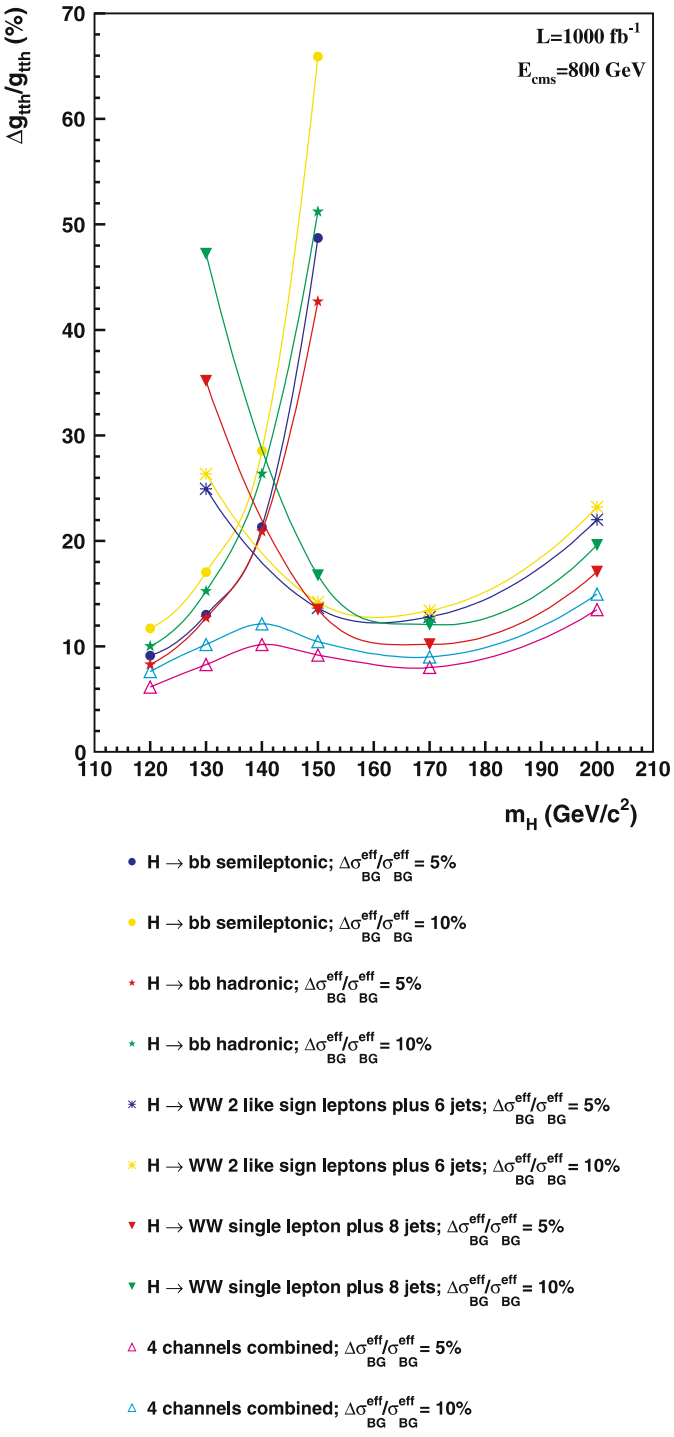

Fig. 4. Expected relative uncertainty on the measurement of $g_{tt\,H}$ via the process $e^+e^- \to t\bar{t}H$ for various channels and their combination, for various Higgs boson masses and for two values of the relative uncertainty on the residual background normalisation

- The total visible mass.
- The number of jets (including possible isolated leptons; JADE algorithm with $y_{\rm cut} = 1.10^{-3}$).
- The thrust.
- The aplanarity.

– The light jet mass.
– The heavy jet mass.
– The second Fox–Wolfram moment $h20$.
– $\sum_{i=1}^{4} P_b^{\rm jet}(i)$.
– $E_{\rm max}^{\rm jet} - E_{\rm min}^{\rm jet}$.

$E_{\rm max(min)}^{\rm jet}$ and the $P_b^{\rm jet}(i)$ are calculated once the event is forced into 8 jets.

4.2.3 Results

We apply the same procedure as for the semileptonic channel (see Sect. 4.1.3). The resolutions on $g_{tt\,H}$ (Fig. 4) range from 8.3% (10.1%) to 42.7% (51.2%) for $\frac{\Delta\sigma_{\rm BG}^{\rm eff}}{\sigma_{\rm BG}^{\rm eff}} = 5\%$ (10%).

5 Study of the $H \to W^+W^-$ decay mode

As shown in the previous section, the measurement of $g_{tt\,H}$ in the $H \to b\bar{b}$ decay mode degrades quite rapidly as the Higgs boson mass increases. The reasons are the drop of the cross-section and even more, the decrease of the branching ratio of the Higgs boson into $b\bar{b}$ for the benefit of the $H \to W^+W^-$ decay. We will thus exploit the latter mode when the Higgs boson is heavier than 140 GeV/c^2, and investigate whether it also improves the accuracy on $g_{tt\,H}$ for lighter Higgs boson masses.

In this decay mode, four intermediate W bosons are present, leading to several classes of final states. Unlike the final states where the Higgs boson decays into a pair of b-quarks, there are only two b-jets in the event, thus the b-tagging is no longer such an essential point of the analysis. Therefore, particular final states have to be identified which can allow good signal and background separation and which provide enough statistical power. Two such channels were found: the "2 like sign lepton plus 6 jet channel", when two W bosons of the same sign decay leptonically while the two remaining ones decay hadronically, and the "single lepton plus 8 jet channel" when only one of the W's decays leptonically. As for channels where the Higgs boson decays into pairs of b-quarks, these final states have large particle and jet multiplicities, an isotropic topology and a tiny event rate. For each channel, the same analysis will be repeated for 4 values of the Higgs boson mass within the range 130–200 GeV/c^2.

5.1 The 2 like sign lepton plus 6 jet channel

The final state follows from the process: $e^+e^- \to t\bar{t}H \to W^+bW^-\bar{b}W^+W^- \to 2l^{\pm}2\nu 2b4q$. Its branching ratio is:

$$\begin{aligned}\mathrm{BR}(t\bar{t}H \to 2l^{\pm}2\nu 2b4q) &= \mathrm{BR}(H \to W^+W^-)\\ &\times \mathrm{BR}(W^{\pm}W^{\pm} \to 4q)\\ &\times \mathrm{BR}(W^{\pm}W^{\pm} \to 2l2\nu) \times 2\\ &\approx 9.6\%\,\mathrm{BR}(H \to W^+W^-)\,.\end{aligned}$$

This channel is thus characterized by a missing 4-momentum, two energetic and isolated charged leptons of the same sign, 4 light quark jets and 2 b-jets. In comparison with the case where no restriction on the charged lepton signs is applied, requiring the two leptons to have the same sign divides the branching ratio of the signal by a factor 3 but the background can be very effectively suppressed.

The analysis will be purely sequential, no neural network being applied.

5.1.1 Analysis

We first apply a set of criteria related to topological variables:

– 400 GeV/c^2 < Total visible mass < 700 GeV/c^2.
– 85 < Total multiplicity < 160.
– Number of jets (including possible isolated leptons; JADE algorithm with $y_{\rm cut} = 1.10^{-3}$) > 6.
– Light jet mass > 100 GeV/c^2.
– Heavy jet mass > 150 GeV/c^2.
– Fox–Wolfram moment h10 < 0.2.
– Fox–Wolfram moment $h20 < 0.45$.
– Fox–Wolfram moment $h30 < 0.3$.
– Fox–Wolfram moment $h40 < 0.3$.

The particles (discarding the charged leptons) of the surviving events are forced into a 6 jet configuration (using JADE) and the jets are flavour-tagged. The events are then required to fulfill the following criteria:

– Minimum dijet invariant mass > 15 GeV/c^2.
– $P_b^{\rm jet}(1) > 0.2$.

The request of only one b-jet allows to preserve a high selection efficiency. Next, we make use of the lepton content of the signal events to further eliminate the background. For each charged lepton reconstructed in the event, we calculate the transverse momentum with respect to the closest jet. Next, we classify the leptons from the most isolated to the least isolated according to this quantity. In the event, there should be 2 and only 2 isolated leptons. Moreover, they should have the same sign. As they come from the primary vertex, the significance of their impact parameter[1] should be small in comparison with the one of a lepton coming from a b- or c-meson decay. Therefore, we require:

– The 2 most isolated leptons have the same sign.
– A p_t between the most isolated lepton and the other jets ≥ 5 GeV/c.
– A p_t between the second most isolated lepton and the other jets ≥ 5 GeV/c.
– A p_t between the third most isolated lepton and the other jets ≤ 5 GeV/c.
– $-0.001 <$ significance[2] of most isolated lepton impact parameter < 0.001.
– $-0.001 <$ significance of second most isolated lepton impact parameter < 0.001.

As the number of signal events is small in this channel but the purity high, the total uncertainty on $g_{tt\,H}$ is

[1] Defined as the distance of closest approach between the track and the primary vertex.

[2] Ratio between the impact parameter and its estimated uncertainty.

dominated by the statistical uncertainty. Therefore, the relative uncertainty on the residual background normalisation has only a modest influence on the total uncertainty. As a matter of fact, the procedure is not reoptimised for each value of the relative uncertainty on the residual background normalisation.

5.1.2 Results

The resolutions on $g_{tt\,H}$ (Fig. 4) range from 12.8% (13.4%) to 24.9% (26.3%) for $\frac{\Delta\sigma^{\rm eff}_{\rm BG}}{\sigma^{\rm eff}_{\rm BG}} = 5\%$ (10%).

5.2 The single lepton plus 8 jet channel

The final state follows from the process: $e^+e^- \to t\bar{t}H \to W^+bW^-\bar{b}W^+W^- \to l\nu 2b6q$. Its branching ratio is:

$$\begin{aligned}\mathrm{BR}(t\bar{t}H \to l\nu 2b6q) &= 4\mathrm{BR}(H \to W^+W^-)\\ &\quad\times \mathrm{BR}(W \to l\nu)\\ &\quad\times (\mathrm{BR}(W \to 2q))^3\\ &\approx 40\%\,\mathrm{BR}(H \to W^+W^-)\,.\end{aligned}$$

This channel is thus characterized by a missing 4-momentum, one prompt charged lepton, 6 light quark jets and 2 b-jets. This signature is less singular than the one of the previous channel but the branching ratio is about 4 times larger. This final state is close to the one of the $H \to b\bar{b}$ semileptonic channel, the analysis will thus be very similar.

5.2.1 Sequential analysis

We first request the presence of at least one charged lepton (a $\mu^\pm$ or a $e^\pm$). Then, we require:

- 500 GeV/c^2 < Total visible mass < 750 GeV/c^2.
- Total multiplicity ≥ 110.
- Number of jets (including possible isolated leptons; JADE algorithm with $y_{\rm cut} = 1.10^{-3}$) ≥ 8.
- Thrust ≤ 0.8
- Fox–Wolfram moment $h10 \leq 0.1$.
- Fox–Wolfram moment $h20 \leq 0.5$.
- Fox–Wolfram moment $h30 \leq 0.3$.
- Fox–Wolfram moment $h40 \leq 0.3$.
- Light jet mass ≥ 100 GeV/c^2.
- Heavy jet mass ≥ 150 GeV/c^2.

To identify an energetic and isolated charged lepton, we proceed as in the $H \to b\bar{b}$ semileptonic channel. The only difference is that, here, to tag the lepton as well as when it has been tagged, the remaining particles are forced to a 8 jet configuration (with the JADE algorithm). The jets are then flavour-tagged and finally we require:

- Mininum jet multiplicity ≥ 3.
- $\sum_{i=1}^{2} P_b^{\rm jet}(i) \geq 0.2$.

5.2.2 Neural network analysis

A neural network is then trained with the following variables:

- The total visible mass.
- The number of jets (including possible isolated leptons; JADE algorithm with $y_{\rm cut} = 1.10^{-3}$).
- The thrust.
- The aplanarity.
- The energy of the tagged lepton.
- The invariant mass of the system made of the lepton and the missing momentum.
- The cosine of the angle between the tagged lepton and the closest jet directions.
- $E^{\rm jet}_{\rm max} - E^{\rm jet}_{\rm min}$.
- Maximum dijet invariant mass−minimum dijet invariant mass.
- The second Fox–Wolfram moment $h20$.
- The light jet mass.
- The heavy jet mass.

The lepton related variables are calculated once the event has been forced to the 1 lepton plus 8 jet configuration, as well as the variables $E^{\rm jet}_{\rm max}$, $E^{\rm jet}_{\rm min}$, maximum dijet invariant mass and minimum dijet invariant mass.

5.2.3 Results

We apply the same procedure as for the $H \to b\bar{b}$ semileptonic channel (see Sect. 4.1.3). The resolutions on $g_{tt\,H}$ (Fig. 4) range from 10.2% (12.1%) to 35.2% (47.2%) for $\frac{\Delta\sigma^{\rm eff}_{\rm BG}}{\sigma^{\rm eff}_{\rm BG}} = 5\%$ (10%).

6 Non resonant 6 fermion production

For the sake of completeness, the loss of resolution on $g_{tt\,H}$ due to non resonant 6 fermion production, which was not taken into account so far, was investigated. The generation of these events being a complicated and very time consuming task, thus leading to rather large uncertainties, we adopted the following procedure. We kept the selection criteria found with the resonant background (which is by far the main background) and the residual contamination from the dominant 6 fermion processes was then estimated. The loss of resolution arising from these events should thus be taken as a rough estimate. This should not matter as the residual 6 fermion background came out to be small.

The 6 fermion process partonic events were generated with WHIZARD V.1.2x[3] [22]. Some of them receiving contributions from the non-resonant background considered in the analysis, some diagrams were removed from the calculation to avoid double counting, keeping however the interference between the resonant and non-resonant diagrams. This short-cut was motivated by the complexity a more correct treatment would introduce; it was justified by the magnitude of the interferences considered. As for $t\bar{t}H$ and $t\bar{t}Z$ events, they were treated with PYTHIA V.6.158 for hadronization, decay and final state radiation. Beamstrahlung and initial state radiation were handled

[3] Versions 1.22 to 1.24 were used.

by WHIZARD. The partonic events were then passed to SIMDET V.4. For each channel studied, the most contaminating 6 fermion processes were identified, produced and their contamination calculated. We observed that the loss of resolution on the measurement of $g_{tt\,H}$ is very modest (i.e. 0.2%–0.7%).

7 Conclusion and outlook

The accuracy achievable on the top-Higgs Yukawa coupling at the linear collider was investigated at a collision energy of 800 GeV for Higgs masses of 120–200 GeV/c^2, assuming an integrated luminosity of 1000 fb^{-1}. The study accounts for all dominant physical backgrounds, the main radiative effects (initial and final state radiation and beamstrahlung) as well as detector and event reconstruction effects. The accuracies obtained include the statistical uncertainty and the systematic uncertainty arising from a limited knowledge of the background normalisation. For Higgs boson masses under $\approx 135\,\mathrm{GeV}/c^2$, the main decay mode is $H \to b\overline{b}$. Two channels were analysed – the hadronic and the semileptonic channels – and we presented the results for the Higgs mass range: 120–150 GeV/c^2. The measurement precision found for a mass of 120 GeV/c^2 in the $H \to b\overline{b}$ mode is slightly worse than in [4], due to refinements of the present analysis which make it more realistic. The resolution degrades with increasing mass, due to the reduced event rate. In this decay mode, the ability to identify b-jets is of major importance. For Higgs boson masses above $\approx 140\,\mathrm{GeV}/c^2$, the $H \to W^+W^-$ decay mode yields higher precision than the $H \to b\overline{b}$ one as the number of signal events in the latter mode becomes too tiny. Two channels were analysed – the 2 like sign lepton plus 6 jet channel and the single lepton plus 8 jet channel – and we presented the results for the Higgs mass range: 130–200 GeV/c^2.

We showed that the 6 fermion background has a very modest influence on the measurement of the coupling.

The question was also addressed whether the present limited knowledge on SM parameters has any significant influence on the expected precision on $g_{tt\,H}$. The largest effect, if any, is expected from the present experimental uncertainty on the top quark mass (which is of the order of 5 GeV/c^2). The analysis of the semileptonic channel (see Sect. 4.1) with $M_\mathrm{H} = 120\,\mathrm{GeV}/c^2$ (for which the change of $\sigma_{t\bar{t}H}$ is the largest) was repeated for $m_t = 170$ and 180 GeV/c^2 and the precision on $g_{tt\,H}$ varied by a negligible amount. The conclusion is therefore that the present accuracy on the SM input parameters has no significant influence on the predicted accuracy on $g_{tt\,H}$.

As a final result, the four channels studied in this paper are combined[4] to get the global precision. The results are displayed in Table 3 and Fig. 4. The expected accuracy on $g_{tt\,H}$ is better than $\approx 10\%$ over most of the mass range (up to $M_\mathrm{H} \approx 180\,\mathrm{GeV}/c^2$), even if the knowledge of the background normalisation is only at the 10% level. In the most favourable case ($M_\mathrm{H} = 120\,\mathrm{GeV}/c^2$ and $\frac{\Delta\sigma^{\mathrm{eff}}_{\mathrm{BG}}}{\sigma^{\mathrm{eff}}_{\mathrm{BG}}} = 5\%$), the accuracy is about 6%. It is also good (8 to 9%) for $M_\mathrm{H} \approx 170\,\mathrm{GeV}/c^2$, corresponding to the maximum of the branching ratio of the Higgs boson into pairs of W's. For the less favourable case ($M_\mathrm{H} = 200\,\mathrm{GeV}/c^2$), the accuracy is however still better than 15% even if $\frac{\Delta\sigma^{\mathrm{eff}}_{\mathrm{BG}}}{\sigma^{\mathrm{eff}}_{\mathrm{BG}}} = 10\%$. We observe that the best resolutions are obtained for the lowest Higgs mass values, which are the most favoured by precision electroweak measurements.

Table 3. Expected relative uncertainty on the measurement of $g_{tt\,H}$ via the process $e^+e^- \to t\bar{t}H$ for the combination of the 4 channels studied, for various Higgs boson masses and for two values of the relative uncertainty on the residual background normalisation

M_H (GeV/c^2)	$\frac{\Delta\sigma^{\mathrm{eff}}_{\mathrm{BG}}}{\sigma^{\mathrm{eff}}_{\mathrm{BG}}}$	$\frac{\Delta g_{tt\,H}}{g_{tt\,H}}$
120	5%	6.1%
	10%	7.6%
130	5%	8.3%
	10%	10.2%
150	5%	9.2%
	10%	10.5%
170	5%	8.0%
	10%	9.0%
200	5%	13.5%
	10%	15.0%

At the LHC, under some conditions which make the analysis more model dependent, the expected accuracy on $g_{tt\,H}$ with 300 fb^{-1} lies in the range 10%–20% for $M_\mathrm{H} \in$ [100–200 GeV/c^2] [23]. The precise measurements of the Higgs branching ratios already available from a low energy run of the linear collider will allow the removal of the model dependency of the LHC results [24]. The achievable accuracies are, however, not as good as those expected from a high energy run of the linear collider.

Finally, it should be stressed that there is certainly room for substantial improvement of the study exposed here. For instance, the b-tagging does not include all observables (e.g. vertex charge), more efficient jet reconstruction and particle flow algorithms could improve the reconstruction, other final states could be included, the reconstruction of τ's could enhance the number of signal events in leptonic channels and the analysis itself (selection criteria, neural network inputs, training and architecture) can also be optimized. Moreover, the analysis may be extended above $M_\mathrm{H} = 200\,\mathrm{GeV}/c^2$ in order to cover the full Higgs mass range allowed by precision measurements.

[4] We combine the uncertainties found without inclusion of 6 fermion processes as the degradation due to them has only been roughly estimated and is anyway small.

Acknowledgements. I thank M. Winter and I. Gornouchkine for valuable discussions.

References

1. ALEPH, DELPHI, L3 and OPAL Collaborations, LEP Working Group for Higgs Boson Searches, Phys. Lett. B **565**, 61 (2003)
2. LEP Electroweak Working Group, http://lepewwg.web.cern.ch/LEPEWWG/
3. H. Baer, S. Dawson, L. Reina, Phys. Rev. D **61**, 013 002 (2000)
4. A. Juste, G. Merino, hep-ph/9910301
5. A. Gay, Ph.D. thesis (Université Louis Pasteur Strasbourg, 2005)
6. A. Gay, LC-PHSM-2006-002, hep-ph/0604034
7. A. Djouadi, J. Kalinowski, M. Spira, Comput. Phys. Commun. **108**, 56 (1998)
8. A. Pukhov et al., hep-ph/9908288
9. A. Juste, hep-ph/0512246
10. S. Dittmaier, M. Kramer, Y. Liao, M. Spira, P. Zerwas, Phys. Lett. B **441**, 383 (1998)
11. S. Dawson, L. Reina, Phys. Rev. D **59**, 054 012 (1999)
12. G. Bélanger et al., hep-ph/0307029
13. C. Farrell, A. Hoang, Phys. Rev. D **72**, 014 007 (2005)
14. T. Sjostrand, L. Lonnblad, S. Mrenna, hep-ph/0108264
15. T. Ohl, Comput. Phys. Commun. **101**, 269 (1997)
16. M. Pohl, H.J. Schreiber, DESY 02-061, LC-DET-2002-005
17. TESLA Technical Design Report, DESY 2001-011, ECFA 2001-209, 2001
18. R. Hawkings, LC-PHSM-2000-021
19. S.M. Xella Hansen, D.J. Jackson, R. Hawkings, C. Damerell, LC-PHSM-2001-024
20. http://flc25.desy.de/flc/science/analysis_ntuple/index.html
21. http://schwind.home.cern.ch/schwind/MLPfit.html
22. W. Kilian, LC-TOOL-2001-039
23. M. Dührssen et al., hep-ph/0406323.
24. K. Desch, M. Schumacher, Eur. Phys. J. C **46**, 527 (2006)